Correlating Defect States with Optical, Dielectric, Electrical, and Mechanical Properties for Ball-Milled $CuAlO_2$

Apurba Sarkar,[1] Soumya Mukherjee,[2#] Chandan Kumar Raul[3], Nandan Pakhira[1]

[1]*Department of Physics, Kazi Nazrul University, Asansol-713340, India*

[2]*Department of Metallurgical Engineering, Kazi Nazrul University, Asansol-713340, India*

[3]*Department of Physics, National Institute of Technology, Durgapur-713209, India*

Abstract: The present study executes a comprehensive evaluation of functional behaviour through detailed optical, dielectric, electrical and mechanical analyses which used to be a follow-up of our previous research work based on structural, thermal & micros-structural features of ball-milled $CuAlO_2$ samples. UV-Vis spectroscopy reveals a direct band gap of 3.82 eV, while photoluminescence exhibits strong blue emission centred at 433 nm, attributed to shallow defect states such as oxygen vacancies and Cu^{+}/Cu^{2+} centres. Dielectric measurements show high permittivity at low frequencies, driven by defect-mediated polarization mechanisms, while I-V characteristics display space-charge-limited conduction governed by trap-assisted hopping. Microhardness testing yields a value of 2.84 GPa, indicating enhanced mechanical stability linked to grain refinement and defect distribution induced by ball milling. The strong correlation between defect states and multifunctional properties-including optical emission, dielectric response, charge transport and mechanical integrity-highlights the role of mechanical activation in tuning $CuAlO_2$ for advanced applications like UV optoelectronics, transparent electronics, and ceramic-based energy devices.

Keywords: $CuAlO_2$, Optical; Dielectric; Defect states; Micro-hardness, I-V characteristics

1. Introduction

Copper-based delafossite oxides particularly $CuAlO_2$, have emerged as promising materials owing to their distinctive combination of wide band gap semi-conductivity, optical transparency, and p-type conductivity. The following functionalities attribute $CuAlO_2$ as a viable candidate for applications in optoelectronic devices, transparent electronics, thermoelectric systems, and photocatalytic platforms [1-3]. Structurally, $CuAlO_2$ crystallizes in a rhombohedral lattice (space group R3m), characterized by linearly coordinated Cu^{+} ions and edge-sharing AlO_6 octahedra. This layered configuration facilitates anisotropic transport and accommodates a range of intrinsic and extrinsic defects, which can significantly influence the material's functional behaviour [4,5].

While different synthesis methods such as sol-gel, hydrothermal and combustion techniques have been employed to prepare $CuAlO_2$ [6-9], mechanical activation via ball-milling offers distinct advantages in terms of particle refinement, defect generation, and phase control. Defect states, particularly oxygen vacancies and mixed-valence copper centres (Cu^{+}/Cu^{2+}) play a pivotal role in modulating the material's optical absorption, photoluminescence, dielectric response, and charge transport mechanisms [10,11]. In our preceding investigation [12], delafossite $CuAlO_2$ is synthesized via a ball milling-assisted solid-state reaction route. The structural phase is confirmed through X-ray diffraction (XRD), revealing the formation of the delafossite phase with high crystallinity. Complementary analyses, including Fourier-transform infrared (FTIR) spectroscopy and scanning electron microscopy (SEM), provided insights into bonding environments and particle morphology, while thermogravimetric analysis (TGA) affirmed the thermal stability of the synthesized material. These characterizations established a robust foundation for further exploration of $CuAlO_2$'s functional properties.

The present study is an extension of our previous investigation by focusing on the optical, dielectric, mechanical, and electrical characteristics of ball-milled $CuAlO_2$ sample. Ultraviolet–visible (UV-Vis) spectroscopy is employed to determine the optical band gap and assess electronic transitions, while photoluminescence (PL) spectroscopy is used to probe defect-related emissions and recombination dynamics. Dielectric measurements across varying frequencies elucidate polarization mechanisms and relaxation behaviour, which are critical for understanding charge storage and transport phenomena. Mechanical integrity is evaluated through Vickers microhardness testing, offering insights into the material's resistance to localized deformation. Additionally, current–voltage (I-V) analysis provides information on charge conduction pathways and defect-mediated transport, enabling a comprehensive understanding of the material's electronic response.

2. Experimental section

2.1 Materials and Methods

The synthesis of $CuAlO_2$ sample from CuO and Al_2O_3 powders via ball milling-assisted solid-state reaction, along with preliminary structural and morphological characterizations (XRD, FTIR, SEM, and EDS), has been comprehensively described in our previous report [12]. In the present study, we extend the characterization to include optical, dielectric, mechanical, and electrical analyses to further elucidate the functional properties of the material.

2.2 Optical characterization

UV-Vis Spectroscopy: The optical absorption spectra were recorded using a UV-Vis spectrophotometer (Agilent Cary 5000 UV-Vis NIR spectrometer) in the wavelength range of 200–800 nm. The absorption edge was analysed using Tauc plot to estimate the optical band gap.

Photoluminescence (PL) Spectroscopy: PL measurement was carried out at room temperature using a fluorescence spectrometer (Horiba FluoroMax 4 Spectrofluorometer) with an excitation wavelength of 330 nm. Emission spectra were recorded in the range of 350-600 nm to investigate defect-related transitions and recombination behaviour.

2.3 Dielectric measurements

Dielectric constant (ε′) was measured using an impedance analyser (Agilent 4294A Precision Impedance Analyzer, Agilent Technologies, Inc. USA) across 100 Hz to 1 MHz. Silver electrodes were applied to sintered pellet for accurate impedance measurements.

2.4 Micro-hardness testing

Vickers microhardness measurements were performed using a microhardness tester (MHT-Smart, Metatech Industries, Pune, India) with a load of 2 N and a dwell time of 10 s. Multiple indentations were made on polished pellet surfaces, and the average diagonal length was used to calculate hardness values using the standard Vickers formula.

2.5 Current-Voltage (I-V) measurements

I-V characteristics were recorded using an electrometer (Keithley 6514) in a two-probe configuration. Silver electrodes were applied to the sintered pellets, and measurements were conducted at room temperature under ambient conditions. The voltage was swept from -15 V to +15 V to evaluate the conduction behaviour and symmetry of the response.

3. Results and discussion

The functional properties of ball-milled $CuAlO_2$ sample were systematically investigated through optical, dielectric, mechanical and electrical analyses. The results reveal strong interdependence between defect states, microstructure and charge transport mechanisms, which collectively govern the material's performance in optoelectronic and energy-related applications.

3.1 Optical properties

3.1.1 UV-Vis reflectance and Band Gap estimation

Fig.1 illustrates the UV-Vis reflectance spectrum obtained for the ball-milled $CuAlO_2$ sample, highlighting its optical response across the measured wavelength range. It exhibits a prominent peak near 350 nm, followed by a gradual decline across the visible region. This behaviour is typical of wide band gap semiconductors, where strong UV absorption arises from electronic transitions between the O-2p dominated valence band and the Cu/Al-derived conduction band [2,4,13]. The sharp reflectance drop beyond the UV region suggests minimal visible light interaction, reinforcing the material's transparency and suitability for optoelectronic applications, including transparent electronics and UV-sensitive devices [1,14].

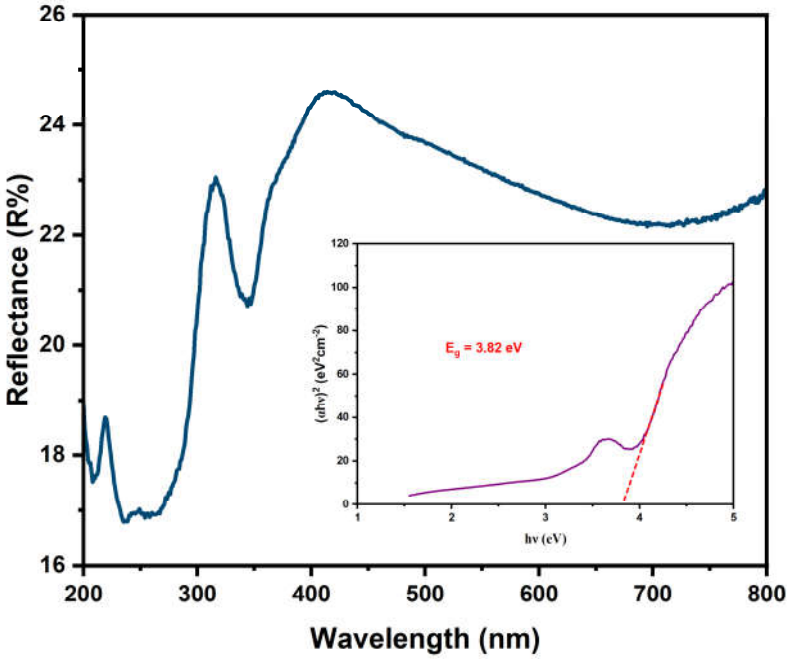

Fig.1. UV-Vis reflectance spectrum of ball-milled $CuAlO_2$ sample showing a sharp absorption edge near 350 nm. The inset displays the Tauc plot used to estimate the direct band gap.

To quantify the optical band gap, a Tauc plot as shown in inset of **Fig.1**, was constructed using the relation $(\alpha h\nu)^2$ vs hν, assuming a direct allowed transition. The extrapolation of the linear region to the energy axis yields a band gap (E_g) of 3.82 eV. This value is slightly higher than typical reports for $CuAlO_2$, which generally range between 3.5-3.7 eV [15,16]. This enhancement is primarily attributed to quantum confinement arising from nanoscale particle dimensions [17], strain-induced band widening due to lattice distortion during high-energy milling [18,19], and a reduced density of structural defects that typically introduce sub-band-gap states [20]. Collectively, these effects contribute to a cleaner absorption edge and improved optical transparency, reinforcing $CuAlO_2$'s potential for UV optoelectronic and transparent thin-film applications.

3.1.2 Photoluminescence (PL) spectroscopy

PL spectrum of $CuAlO_2$ at room temperature is shown in **Fig. 2**, reveals a sharp emission peak centred at 433 nm with an intensity of approximately $6x10^6$ in a.u. This emission is attributed to radiative recombination involving shallow defect states, primarily oxygen vacancies and Cu^+/Cu^{2+} centres, which introduce localized energy levels near the conduction band edge [10,21]. The absence of broad or red-shifted emissions indicates a low density of deep-level defects, suggesting high crystallinity and minimal non-radiative recombination pathways [4,11].

The sharp PL response reflects efficient band-edge transitions, which are essential for optoelectronic devices such as UV photodetectors and transparent conductors. Similar defect-

mediated luminescence has been reported in other delafossite-type oxides, where controlled defect chemistry plays a pivotal role in tuning optical properties and enhancement of device performance [22-24].

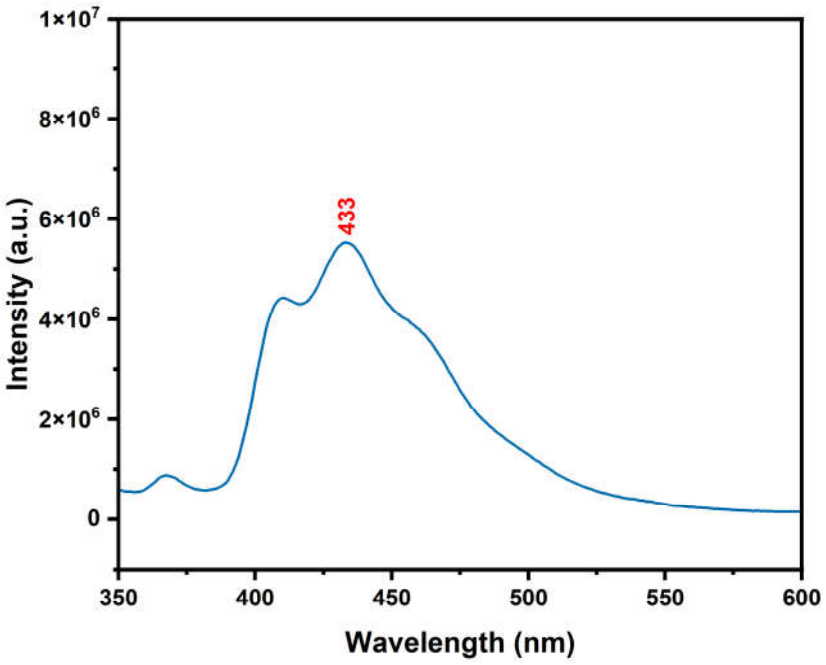

Fig. 2. Photoluminescence spectrum of $CuAlO_2$ sample recorded at room temperature.

3.2 Dielectric analysis

The frequency-dependent dielectric constant (ε') of $CuAlO_2$, as illustrated in **Fig. 3**, exhibits pronounced dispersion, decreasing from approximately 700 at low frequencies ($Log_{10}(f) \approx 2$ Hz) to around 200 at higher frequencies ($Log_{10}(f) \approx 3$ Hz), beyond which it stabilizes. This behaviour reflects the influence of multiple polarization mechanisms, notably space charge, dipolar, and interfacial polarization, which are active at low frequencies and progressively diminish with increasing frequency [25].

At low frequencies, the elevated ε' values are attributed to defect-related polarization, where mobile charge carriers and localized defect states interact with the applied electric field. At higher frequencies, inertial impact due to effective higher masses of electron cloud, coupled with intrinsic dipolar polarization impact with frequency application leads to slower response. The high dielectric constant at low frequencies also suggests potential for energy storage and capacitive applications, where interfacial polarization enhances charge accumulation [26].

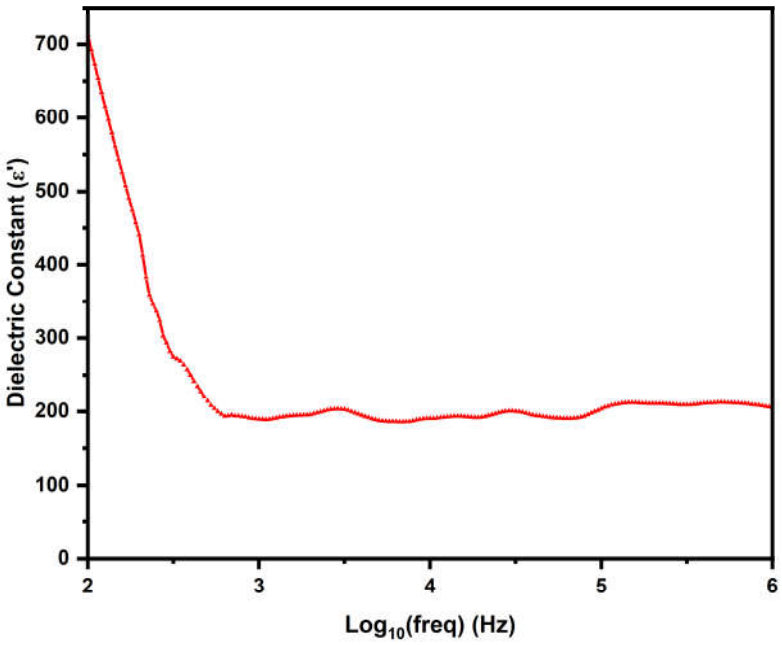

Fig. 3. Frequency dependent dielectric constant (ε') of as-synthesized $CuAlO_2$ sample at room temperature.

These findings complement the PL results, as both suggest the presence of shallow defect states that influence polarization dynamics. The correlation between optical and dielectric behaviour legitimised the multifunctional nature of $CuAlO_2$.

3.3 Mechanical properties

Microhardness testing is obtained from the Vickers indentation method which yields a hardness value of 2.84 GPa for the ball-milled $CuAlO_2$ sample. This value reflects moderate mechanical strength, suitable for integration into thin-film devices and layered heterostructures, where mechanical resilience and dimensional stability are critical [8]. The corresponding microstructural image, as shown in inset in **Fig.4**, reveals dense and uniform grain morphology with minimal porosity and well-defined grain boundaries. Such features enhance mechanical integrity by improving load distribution and inhibiting crack propagation, thereby improving the material's resistance to localized deformation and fracture [27,28].

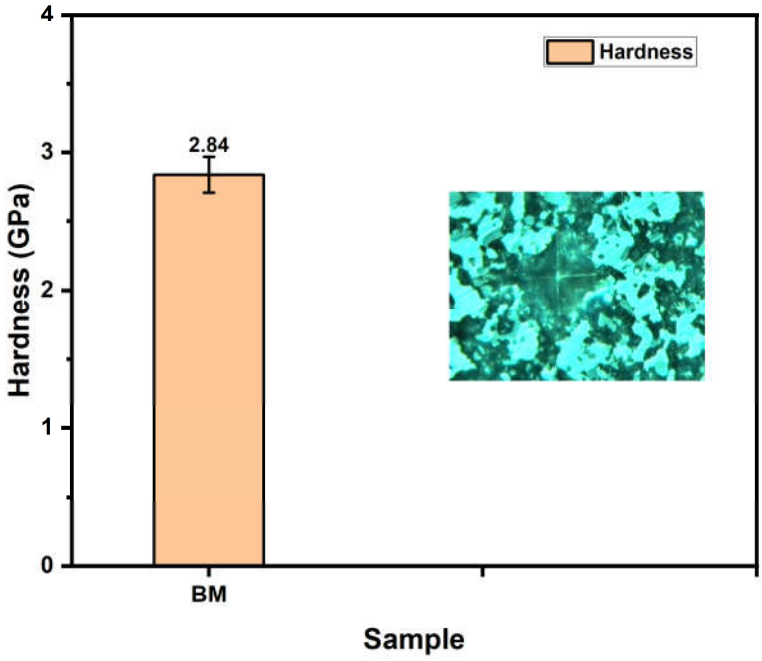

Fig.4. Vickers microhardness profile of ball-milled $CuAlO_2$ pellets, with an average hardness value of 2.84 GPa. The inset shows the indentation pattern confirming uniform load distribution and mechanical integrity.

Grain refinement induced by ball milling contributes to the observed hardness, as smaller grains increase the number of grain boundaries, which act as barriers to dislocation motion, a phenomenon consistent with the Hall-Petch effect [29]. The mechanical robustness of $CuAlO_2$ is particularly advantageous for applications requiring structural stability under thermal and electrical stress, such as transparent electrodes and thermoelectric modules.

3.4 Electrical Properties (I-V characteristics)

The current-voltage (I-V) characteristics of $CuAlO_2$, measured over a voltage range of -15 V to +15 V, as illustrated in **Fig. 5**, exhibit a symmetric and non-linear profile. At voltages below -10 V and above +10 V, the current saturates at approximately ±0.010 µA, while within the intermediate range (-10 V to +10 V), the current increases gradually. This behaviour is indicative of space-charge-limited conduction (SCLC), where charge transport is governed by trap-assisted hopping and defect-mediated pathways [30].

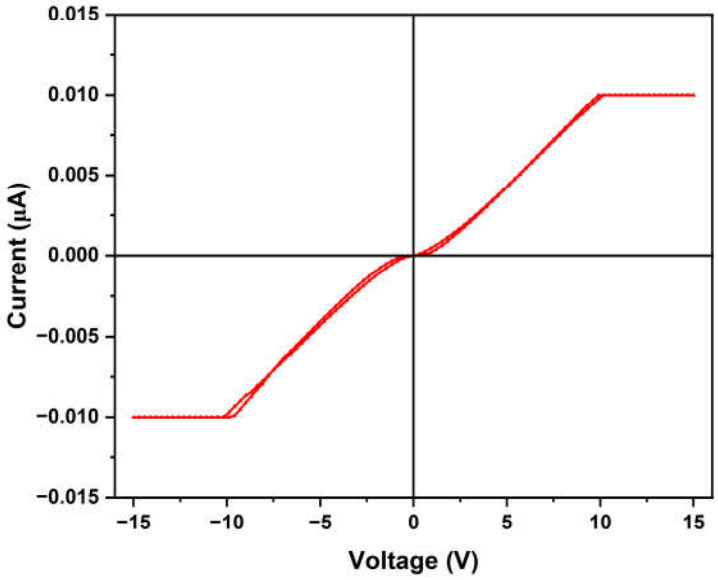

Fig.5. Current-voltage (I-V) characteristics of $CuAlO_2$ sample measured over ±15 V, showing symmetric and non-linear behaviour consistent with space-charge-limited conduction and trap-assisted transport.

At low voltages, injected carriers are captured by trap states, leading to a sub-linear increase in current. As the voltage increases, these traps become filled, and the current approaches a steady-state regime. The symmetric nature of the curve suggests ohmic contact behaviour, with minimal barrier formation at the electrode-sample interface.

The low current magnitude, in the microampere range, is consistent with the wide band gap and low intrinsic carrier concentration of $CuAlO_2$. The correlation between PL emissions and I-V behaviour reinforces the role of shallow defect states in facilitating charge transport. Additionally, the dielectric analysis supports this interpretation, as polarization mechanisms can influence carrier mobility and trap dynamics.

Collectively, these results highlight the potential of $CuAlO_2$ for low-power electronic and optoelectronic applications, where defect engineering can be strategically employed to tailor conductivity and switching behaviour.

4. Conclusions

The present article provides investigation into ball-milled $CuAlO_2$ nanoparticles in terms of functional properties, complementing earlier structural and thermal analyses. The material demonstrates a wide optical band gap of 3.82 eV and distinct blue photoluminescence around 433 nm, both arising from intrinsic defect states such as oxygen vacancies and mixed-valence copper centres. Dielectric studies reveal elevated permittivity at low frequencies, attributed to defect-induced polarization effects, while electrical measurements show non-linear, symmetric I-V behaviour consistent with space-charge-limited conduction. Additionally, microhardness testing indicates a value of 2.84 GPa, suggesting improved mechanical resilience linked to grain refinement and defect distribution from the ball milling process. By

integrating these functional characterizations, the study provide a holistic assessment of $CuAlO_2$ synthesized via ball milling, underscoring the role of defect engineering for property manifestation. The material demonstrates promising potential for integration into UV optoelectronic devices, transparent conductors, and ceramic-based energy applications future work.

Conflicts of interest

The authors declare no competing interests.

Acknowledgements

The authors sincerely thank **IIT Kharagpur**, **Jadavpur University**, **NIT Durgapur**, and **Kazi Nazrul University** for providing essential research infrastructure and institutional support. One of the authors (**AS**) gratefully acknowledges the **CSIR-UGC**, Government of India, for the award of a **Senior Research Fellowship (SRF)**, which supported this work. The team also extends appreciation to all collaborators and technical personnel for their meaningful contributions throughout the research.

References

[1] Kawazoe, H., Yasukawa, M., Hyodo, H., Kurita, M., Yanagi, H., & Hosono, H. (1997). P-type electrical conduction in transparent thin films of CuAlO2. *Nature*, *389*(6654), 939-942. https://doi.org/10.1038/40087.

[2] Yanagi, H., Inoue, S. I., Ueda, K., Kawazoe, H., Hosono, H., & Hamada, N. (2000). Electronic structure and optoelectronic properties of transparent p-type conducting CuAlO 2. *Journal of Applied Physics*, *88*(7), 4159-4163. https://doi.org/10.1063/1.1308103.

[3] Guarneros Aguilar, C., Estrada Moreno, C., Pacio Castillo, M., & Caballero-Briones, F. (2018). Effect of calcination temperature on structure and thermoelectric properties of CuAlO2 powders. *Journal of Materials Science*, *53*(3), 1646-1657. https://doi.org/10.1007/s10853-017-1602-8.

[4] Pellicer-Porres, J., Segura, A., Gilliland, A. S., Munoz, A., Rodríguez-Hernández, P., Kim, D., ... & Kim, T. Y. (2006). On the band gap of CuAlO2 delafossite. *Applied physics letters*, *88*(18). https://doi.org/10.1063/1.2200398.

[5] Ingram, B. J., González, G. B., Mason, T. O., Shahriari, D. Y., Barnabe, A., Ko, D., & Poeppelmeier, K. R. (2004). Transport and defect mechanisms in cuprous delafossites. 1. Comparison of hydrothermal and standard solid-state synthesis in CuAlO2. *Chemistry of materials*, *16*(26), 5616-5622. https://doi.org/10.1021/cm048983c.

[6] Benreguia, N., Barnabé, A., & Trari, M. (2015). Sol–gel synthesis and characterization of the delafossite CuAlO2. *Journal of Sol-Gel Science and Technology*, *75*(3), 670-679. https://doi.org/10.1007/s10971-015-3737-x.

[7] Shahriari, D. Y., Barnabe, A., Mason, T. O., & Poeppelmeier, K. R. (2001). A high-yield hydrothermal preparation of CuAlO2. *Inorganic chemistry*, *40*(23), 5734-5735. https://doi.org/10.1021/ic015556h.

[8] Khedidji, M., Saib, F., Mahroua, O., & Trari, M. (2022). The structural, electronic, magnetic, optical and vibrational properties of the delafossite CuAlO2: DFT calculations and experimental study. *Journal of Materials Science: Materials in Electronics*, *33*(35), 26474-26483. https://doi.org/10.1007/s10854-022-09326-y.

[9] Mukherjee, S. (2025). Evolution of delafossite $CuAlO_2$ by sol-gel process and its characterizations. *Zhuzao/Foundry, 28(6), 75-79.* https://doi.org/10.29014/FJ-2025-1001-4977.89.2059.

[10] Banerjee, A. N., Ghosh, C. K., & Chattopadhyay, K. K. (2005). Effect of excess oxygen on the electrical properties of transparent p-type conducting CuAlO2+ x thin films. *Solar energy materials and solar cells*, *89*(1), 75-83. https://doi.org/10.1016/j.solmat.2005.01.003.

[11] Gunkel, F., Christensen, D. V., Chen, Y. Z., & Pryds, N. (2020). Oxygen vacancies: The (in) visible friend of oxide electronics. *Applied physics letters*, *116*(12). https://doi.org/10.1063/1.5143309.

[12] Sarkar, A., Mukherjee, S., Pakhira, N. (2025). Characterization of CuAlO2 Synthesized by ball milling assisted process in terms of Thermal, Structural, Morphological and Spectroscopic Analyses. *Zhuzao/Foundry, 28(7), 70-80.* https://doi.org/10.29014/FJ-2025-1001-4977.89.2081

[13] Kawazoe, H., Yanagi, H., Ueda, K., & Hosono, H. (2000). Transparent p-type conducting oxides: design and fabrication of pn heterojunctions. *Mrs Bulletin*, *25*(8), 28-36. https://doi.org/10.1557/mrs2000.148.

[14] Ismail, R. A., Rashid, F. F., & Tariq, M. S. (2017). Preparation and characteristics study of CuAlO2/Si heterojunction photodetector by pulsed laser deposition. *Journal of Materials Science: Materials in Electronics*, *28*(9), 6889-6896. https://doi.org/10.1007/s10854-017-6389-5.

[15] Banerjee, A. N., Joo, S. W., & Min, B. K. (2012). Quantum size effect in the photoluminescence properties of p-type semiconducting transparent $CuAlO_2$ nanoparticles. *Journal of Applied Physics, 112*(11), 114329. https://doi.org/10.1063/1.4768933.

[16] Ghosh, C. K., Popuri, S. R., Sarkar, D., & Chattopadhyay, K. K. (2011). Sb-doped $CuAlO_2$: Widening of band gap and nonlinear J–E characteristics. *Journal of Materials Science, 46*(6), 1613–1621. https://doi.org/10.1007/s10853-010-4975-5

[17] Brus, L. E. (1984). Electron–electron and electron-hole interactions in small semiconductor crystallites. *Journal of Chemical Physics, 80*(9), 4403–4409. https://doi.org/10.1063/1.447218.

[18] Koreishi, K., Onuma, T., Soma, T., & Ohtomo, A. (2025). Strain-induced band-gap widening in (100) thin films grown on buffer layers. *Physical Review Materials, 9*(L031601). https://doi.org/10.1103/PhysRevMaterials.9.L031601.

[19] Sun, Y., Wong, K. H., & Kwok, K. W. (2021). Strain-induced band gap tuning in flexible ferroelectric/mica thin films. *Thin Solid Films, 731*, 138741. https://doi.org/10.1016/j.tsf.2021.138741.

[20] Lany, S., & Zunger, A. (2008). Assessment of correction methods for the band-gap problem in defect calculations. *Physical Review B, 78*(23), 235104. https://doi.org/10.1103/PhysRevB.78.235104.

[21] Scanlon, D. O., Walsh, A., & Watson, G. W. (2009). Understanding the p-type conduction properties of the transparent conducting oxide CuBO2: a density functional theory analysis. *Chemistry of Materials*, *21*(19), 4568-4576. https://doi.org/10.1021/cm9015113.

[22] Khedidji, M., Saib, F., Mahroua, O., & Trari, M. (2022). The structural, electronic, magnetic, optical and vibrational properties of the delafossite CuAlO2: DFT calculations and experimental study. *Journal of Materials Science: Materials in Electronics*, *33*(35), 26474-26483. https://doi.org/10.1007/s10854-022-09326-y.

[23] Ingram, B. J., González, G. B., Mason, T. O., Shahriari, D. Y., Barnabe, A., Ko, D., & Poeppelmeier, K. R. (2004). Transport and defect mechanisms in cuprous delafossites. 1. Comparison of hydrothermal and standard solid-state synthesis in CuAlO2. *Chemistry of materials*, *16*(26), 5616-5622. https://doi.org/10.1021/cm048983c.

[24] Ingram, B. J., Harder, B. J., Hrabe, N. W., Mason, T. O., & Poeppelmeier, K. R. (2004). Transport and defect mechanisms in cuprous delafossites. 2. CuScO2 and CuYO2. *Chemistry of materials*, *16*(26), 5623-5629. https://doi.org/10.1021/cm048982k.

[25] Prakash, T., Prasad, K. P., Kavitha, R., Ramasamy, S., & Murty, B. S. (2007). *Dielectric relaxation studies of nanocrystalline $CuAlO_2$ using modulus formalism*. Journal of Applied Physics, 102(10), 104104. https://doi.org/10.1063/1.2815633.

[26] Choudhary, N., et al. (2018). *Comprehensive studies of temperature and frequency dependent dielectric and a.c. conducting parameters in third generation multi-component glasses*. RSC Advances, 8, 25468–25479. https://doi.org/10.1039/C8RA04214D.

[27] Broitman, E. (2017). Indentation hardness measurements at macro-, micro-, and nanoscale: a critical overview. *Tribology Letters*, *65*(1), 23. https://doi.org/10.1007/s11249-016-0805-5.

[28] Liu, K., & Wu, J. (2016). Mechanical properties of two-dimensional materials and heterostructures. *Journal of Materials Research*, *31*(7), 832-844. https://doi.org/10.1557/jmr.2015.324.

[29] Hall, E. O. (1951). The deformation and ageing of mild steel: III discussion of results. *Proceedings of the Physical Society. Section B*, *64*(9), 747.https://doi.org/10.1088/0370-1301/64/9/303.

[30] Mott, N. F., & Davis, E. A. (2012). *Electronic processes in non-crystalline materials*. OUP Oxford.